J Biomol NMR (2008) 40:83–94
DOI 10.1007/s10858-007-9212-4

ARTICLE

Comparison of alignment tensors generated for native tRNA^{Val} using magnetic fields and liquid crystalline media

Michael P. Latham · Paul Hanson · Darin J. Brown · Arthur Pardi

Received: 14 August 2007 / Accepted: 24 October 2007 / Published online: 17 November 2007
© Springer Science+Business Media B.V. 2007

Abstract Residual dipolar couplings (RDCs) complement standard NOE distance and J-coupling torsion angle data to improve the local and global structure of biomolecules in solution. One powerful application of RDCs is for domain orientation studies, which are especially valuable for structural studies of nucleic acids, where the local structure of a double helix is readily modeled and the orientations of the helical domains can then be determined from RDC data. However, RDCs obtained from only one alignment media generally result in degenerate solutions for the orientation of multiple domains. In protein systems, different alignment media are typically used to eliminate this orientational degeneracy, where the combination of RDCs from two (or more) independent alignment tensors can be used to overcome this degeneracy. It is demonstrated here for native *E. coli* tRNA^{Val} that many of the commonly used liquid crystalline alignment media result in very similar alignment tensors, which do not eliminate the 4-fold degeneracy for orienting the two helical domains in tRNA. The intrinsic magnetic susceptibility anisotropy (MSA) of the nucleobases in tRNA^{Val} was also used to obtain RDCs for magnetic alignment at 800 and 900 MHz. While these RDCs yield a different alignment tensor, the specific orientation of this tensor combined with the high rhombicity for the tensors in the liquid crystalline media only eliminates two of the four degenerate orientations for tRNA^{Val}. Simulations are used to show that, in optimal cases, the combination of RDCs obtained from liquid crystalline medium and MSA-induced alignment can be used to obtain a unique orientation for the two helical domains in tRNA^{Val}.

Keywords Alignment tensor · Liquid crystalline medium · Magnetic susceptibility anisotropy · RDC · RNA · Domain orientation

Electronic supplementary material The online version of this article (doi:10.1007/s10858-007-9212-4) contains supplementary material, which is available to authorized users.

M. P. Latham · P. Hanson · D. J. Brown · A. Pardi (✉)
Department of Chemistry and Biochemistry, 215 UCB, University of Colorado, Boulder, Boulder, CO 80309-0215, USA
e-mail: arthur.pardi@colorado.edu

Present Address:
D. J. Brown
Department of Biochemistry, University of Colorado at Denver, Health Science Center, MS 8101, P.O. Box 6511, Aurora, CO 80045, USA

Introduction

NMR solution structures are traditionally determined by short-range ^{1}H-^{1}H NOE distance and torsion angle restraints. However, the low density of protons and the non-globular extended structures of many nucleic acids lead to less well-defined structures compared to the NMR solution structures of similar sized proteins. Advances in methodologies for generating tunable alignment of molecules have made it possible to routinely measure residual dipolar couplings (RDCs), which represent valuable structural data for improving the accuracy and precision of NMR solution structures of macromolecules (Tolman et al. 1995; Tjandra and Bax 1997; Bax et al. 2001). Easily measured one-bond ^{1}H-^{15}N and ^{1}H-^{13}C RDCs provide long-range orientational information that complements the local structural restraints provided by NOE and torsion angle data (Tolman et al. 1995; Bax 2003; Lipsitz and Tjandra 2004). Inclusion of RDC data can significantly improve the precision of DNA and RNA structures

(Vermeulen et al. 2000; Padrta et al. 2002; Staple and Butcher 2003; Lipsitz and Tjandra 2004; Davis et al. 2005; Latham et al. 2005; Richards et al. 2006).

Many different external alignment media have been developed to generate the anisotropic molecular orientation required for the observation of RDCs. Currently, the most popular alignment media employed in studies of proteins and nucleic acids are dilute lyotropic liquid crystalline suspensions of bicelles, bacteriophages, or bilayers (Tjandra and Bax 1997; Clore et al. 1998; Hansen et al. 1998; Ruckert and Otting 2000) or anisotropically strained polyacrylamide gels (Sass et al. 2000; Tycko et al. 2000). These external alignment media produce partial alignment of molecules by steric exclusion and/or electrostatic repulsion mechanisms. The intrinsic magnetic susceptibility anisotropy (MSA) of a molecule can also be used to impart partial alignment at higher magnetic fields, therefore allowing measurement of RDCs in the absence of any external medium (Gayathri et al. 1982; Bothner-By 1995). Since the magnitude of MSA-induced alignment scales with the square of the magnetic field, RDCs can be obtained from NMR measurements at two or more magnetic fields (Bothner-By 1995). Extended DNA or RNA helical regions have a significant magnetic anisotropy resulting in partial alignment in high magnetic field. Thus MSA-induced RDCs represent a complementary approach to external alignment media for obtaining long-range orientation restraints in nucleic acids.

Several methods have been developed for determining the low-resolution global structures of nucleic acids including: fluorescence resonance energy transfer and transient electric birefringence (Amiri and Hagerman 1994; Friederich and Hagerman 1997; Lilley 2004). RDCs can also be used to generate global structures of nucleic acids. This approach assumes A-form or B-form structures for the helical domains; rigid body rotations are then performed to find domain orientations that give good fits to the RDC data (Mollova et al. 2000; Bondensgaard et al. 2002; Lukavsky et al. 2003; van Buuren et al. 2004; Vermeulen et al. 2005; Getz et al. 2007). In this analysis since the local structure of helical domains is fixed, the global structures can be determined from a relatively small number of RDCs (Mollova et al. 2000). One-bond ^{1}H-^{15}N imino RDCs ($^{1}D_{HN}$) are particularly useful for domain orientation studies of ^{15}N-labeled RNAs because the imino protons are usually well resolved, readily assigned and generally yield one orientational constraint for each Watson–Crick base pair. A complication with this method is that the RDC is a multivalued function of the angles of the vector between the two nuclei involved in the RDC and the alignment tensor of the molecule (Bax 2003). This leads to 4^{n-1} degenerate solutions for orienting n domains using only RDC data (Bruschweiler et al. 1995; Lipsitz and Tjandra 2004). This orientational degeneracy can be lifted if RDCs are measured for independent alignment tensors. Multiple external alignment media can be employed to try to find an independent alignment tensor for the molecule (Al-Hashimi et al. 2000). This method has been employed in domain orientation studies of protein systems (Al-Hashimi et al. 2000; Lipsitz and Tjandra 2004). The combination of external alignment media and MSA-induced alignment has also been used to orient domains in a homodimeric DNA quadraplex containing a C2 axis of symmetry (Al-Hashimi et al. 2001).

Here we demonstrate that the most commonly used liquid crystalline alignment media give very similar alignment tensors for native *E. coli* tRNA^{Val} (Fig. 1). These media include: filamentous bacteriophages Pf1 (Hansen et al. 1998) and fd (Clore et al. 1998), C_8E_5/*n*-octanol bilayers (Ruckert and Otting 2000), phospholipid bicelles composed of DMPC/DHPC (Tjandra and Bax 1997) and anionic SDS-doped bicelles (Losonczi and Prestegard 1998; Ramirez and Bax 1998). We also show that magnetic alignment of native *E. coli* tRNA^{Val} leads to a different alignment tensor than that observed for the external alignment media. These data can be used to eliminate two of the four degenerate structures generated in domain orientations studies of tRNA^{Val}. However, the other two structures give nearly identical fits to the MSA-induced RDCs illustrating that although the alignment tensors are different, they are not independent. Simulations are performed to determine whether additional RDC data and/or different properties of the alignment tensor would make it possible to determine the correct orientation of the helical domains in tRNA^{Val}.

Materials and methods

Preparation of ^{15}N-labeled tRNA^{Val}

^{15}N-labeled native *E. coli* tRNA^{Val} (Fig. 1) was overexpressed in *E. coli* (BL21(DE3)) from the pVALT7 plasmid in M9 minimal media containing $^{15}NH_4Cl$ as the sole nitrogen source and purified as previously described (Yue 1994; Vermeulen 2003). After purification, tRNA^{Val} samples were extensively dialyzed into NMR buffer (10 mM sodium phosphate, pH 6.8, 80 mM NaCl, 5 mM $MgCl_2$ and 0.1 mM EDTA in 10% D_2O/90% H_2O) by repeated centrifugation in Centricon YM-10 centrifugal filter devices (Millipore, Bedford, MA) and stored at −20°C.

RDCs from external alignment media

The filamentous bacteriophage fd (Clore et al. 1998) and a 20% longer fd phage, fd-9ah8, were purified using a similar

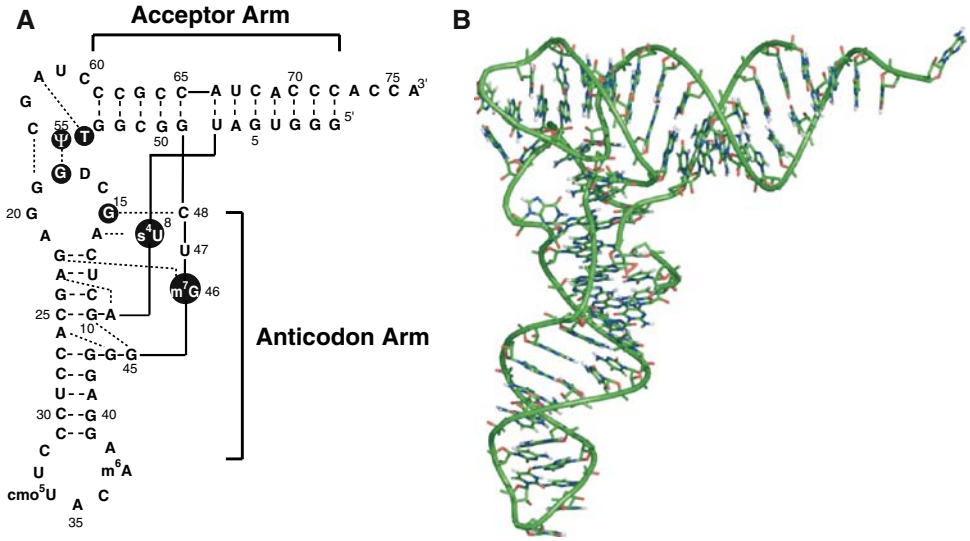

Fig. 1 (**a**) Sequence and secondary structure and (**b**) tertiary structure model of native *E. coli* $tRNA^{Val}$ (Vermeulen et al. 2005). (**a**) Long dashes represent canonical Watson–Crick base pairs and the short dashed lines represent non-canonical or tertiary interactions. Imino groups of the residues in black circles are involved in tertiary interactions, and their $^1D_{HN}$ values were omitted from SVD analysis. The two helical domains are labeled as the acceptor arm and the anticodon arm

procedure to that employed for Pf1 (Hansen et al. 2000). NMR samples were prepared by adding a concentrated stock solution of phage to ^{15}N-labeled $tRNA^{Val}$. For phospholipid bicelles, a DMPC/DHPC stock solution containing a total lipid concentration of 15% w/v (q = 3.5:1.0) was prepared in 10 mM sodium phosphate, pH 7.0, 80 mM NaCl, 5 mM $MgCl_2$ and 0.5 mM EDTA (Tjandra and Bax 1997). Negatively charged bicelles were prepared by adding SDS from a 10% w/v stock solution to the 15% w/v solution of DMPC/DHPC to give a 58:1 ratio of DMPC:DHPC:SDS (q = 3.5:1:0.06) (Losonczi and Prestegard 1998; Ramirez and Bax 1998). NMR samples were made by adding the DMPC/DHPC or DMPC/DHPC/SDS stock solutions to ^{15}N-labeled $tRNA^{Val}$ to a final lipid concentration of 5% w/v.

NMR data on $tRNA^{Val}$ samples in the presence and absence of external alignment media were acquired on Varian Inova 500 and 600 spectrometers (Varian, Inc.) equipped with triple resonance z-axis pulsed field gradient probes. Some data collected at 600 MHz were acquired with a Varian triple resonance z-axis gradient cryogenic probe. The ^{1}H-^{15}N couplings for observable imino groups in $tRNA^{Val}$ were measured utilizing 2D ^{1}H-coupled gradient-selected, sensitivity-enhanced ^{1}H, ^{15}N HSQC (Piotto et al. 1992) or 2D doublet-selective sensitivity-enhanced ^{1}H, ^{15}N HSQC (Cordier et al. 1999) experiments. The ^{1}H-^{15}N couplings for the unaligned $tRNA^{Val}$ ($^1J_{HN}$) were measured at 25°C on a sample with no external media, whereas the couplings for the aligned states ($^1J_{HN}$ + $^1D_{HN}$) were collected at 25°C for the fd phage and at 38°C for the two DMPC/DHPC media. All NMR data were processed and analyzed with NMRPipe/NMRDraw software (Delaglio et al. 1995). The ^{1}H and ^{15}N resonance assignments for the imino groups of $tRNA^{Val}$ were based on previously published values (Mollova et al. 2000; Vermeulen et al. 2005). The ^{1}H-^{15}N imino RDCs ($^1D_{HN}$) resulting from alignment by external alignment media were determined by subtracting the measured couplings in the unaligned state from those in the aligned state.

RDCs from magnetic alignment

The one-bond ^{1}H-^{15}N imino couplings, $^1J_{HN}(B_0)$, were measured at 25°C at four magnetic fields using Varian Inova 500, 600 and 800 and VNMRS 900 spectrometers. These couplings were averaged from two independent data sets (Ying et al. 2007) where for the first data set the couplings were directly measured from peak splittings in a ^{1}H-coupled ^{1}H, ^{15}N HSQC spectrum (Piotto et al. 1992) and for the second data set the couplings were calculated by doubling the measured difference in peaks positions in two separately acquired spectra: a decoupled ^{1}H, ^{15}N HSQC spectrum and a TROSY-HSQC (Pervushin et al. 1997) spectrum. The $^1D_{HN}(B_0)$ values for magnetic alignment were determined by first calculating the zero-field one-bond coupling constant ($^1J_{HN}(0)$), which is the intercept of the best-fit line of $^1J_{HN}(B_0)$ versus B_0^2 (Bothner-By 1995). A weighted least squares method was used to calculate $^1J_{HN}(0)$ with the inverse of the average pairwise root mean square difference (rmsd) of the two data sets collected at each magnetic field used as the weighting factor in the linear regression. $^1D_{HN}(800)$ and $^1D_{HN}(900)$ values were then determined by subtracting $^1J_{HN}(0)$ from $^1J_{HN}(800)$ or $^1J_{HN}(900)$, respectively. In some of the analysis the $^1D_{HN}(800)$ and $^1D_{HN}(900)$ values were combined to obtain a normalized average value, referred to as $^1D_{HN}(800, 900)$, which is equal to $[^1D_{HN}(800) + (800^2/900^2)^1D_{HN}(900)]/2$.

Determination of alignment tensors for tRNA^{Val}

The singular value decomposition (SVD) approach was used to calculate the alignment tensor for native *E. coli* tRNA^{Val} for the different alignment conditions (Losonczi et al. 1999; Sass et al. 1999). The previously determined rigid-body minimized, domain-oriented structure of native *E. coli* tRNA^{Val} (Vermeulen et al. 2005) and the experimental $^{1}D_{HN}$ values for a given alignment condition were used as input for the SVD program REDCAT (Valafar and Prestegard 2004). The observed $^{1}D_{HN}$ for imino groups from residues involved in tertiary interactions (s^4U8, G15, G18, m^7G46, T54 and Ψ55, see Fig. 1a) were excluded in the SVD analysis of the alignment tensor. The REDCAT program uses a Monte-Carlo approach, which performs multiple SVD fits and assumes Gaussian errors for the RDCs (Valafar and Prestegard 2004). The program only generates a solution when all the back-calculated RDCs are within the input error. Initial SVD calculations using the experimental errors in the RDCs (±1.5 Hz) as the input error for REDCAT resulted in no solutions for the RDC data from Pf1, C_8E_5/1-octanol bilayer or DMPC/DHPC bicelles. This is because there is "structural noise" in the local structure of the native *E. coli* tRNA^{Val} model (Zweckstetter and Bax 2002; Vermeulen et al. 2005), which results from helical regions being constructed assuming canonical A-form helices (Vermeulen et al. 2005). Thus for the media that have higher degrees of alignment, larger errors on the RDCs were used for the SVD calculations to account for the systematic error arising from structural noise (±2, ±5, ±5 and ±6 Hz for the fd-8ah8, Pf1, C_8E_5/1-octanol bilayer and DMPC/DHPC bicelles, respectively). A total of 10^3–10^4 SVD calculations were performed with these input errors which led to 70–80% of the calculations producing solutions that fit the input RDC data (Zweckstetter and Bax 2002).

Results and discussion

Different external alignment media yield similar alignment tensors

The imino $^{1}D_{HN}$ values were measured for native *E. coli* tRNA^{Val} (Fig. 1) in the following external liquid crystalline alignment media: 20 mg/ml wt-fd phage, 20 mg/ml fd-9ah8 phage, 5% DMPC/DHPC bicelles and SDS-doped 5% DMPC/DHPC bicelles (Table S1). The $^{1}D_{HN}$ values for this tRNA were previously measured in two other alignment media: 10 mg/ml Pf1 phage (Mollova et al. 2000) and 3.5% C_8E_5/1-octanol bilayers (Vermeulen et al. 2005). Figure 2a shows a scatter plot of $^{1}D_{HN}$ values for the two different lengths of fd phage versus $^{1}D_{HN}$ values from Pf1. Since the Pf1 and fd phage have similar negatively charged filamentous structures, it is not surprising that there is a very high degree of correlation between RDCs for tRNA^{Val} in these phage media. Figure 2b shows a scatter plot of the $^{1}D_{HN}$ values for the bicelle and bilayer media versus the $^{1}D_{HN}$ values for Pf1, and these plots also show a high correlation between the RDC data sets. Except for the SDS-doped DMPC/DHPC bicelles, the scatter plots for all the media have Pearson's correlation coefficients (R_P) ranging from 0.90 to 0.98 indicating strong linear correlations (Fig. 2 and Table S1). Strong linear correlations in these scatter plots indicate that the alignment tensors of tRNA^{Val} in these other media are very similar to the tensor in Pf1 phage. The higher degree of alignment of tRNA^{Val} in the DMPC/DHPC bicelles leads to additional ^{1}H-^{1}H RDCs, which causes the apparent line-broadening for many of the ^{1}H-^{15}N imino resonances in the NMR spectrum of tRNA^{Val} (Fig. 3a). Thus only 14 $^{1}D_{HN}$ values could be measured in the DMPC/DHPC bicelles compared to the 26–27 $^{1}D_{HN}$ values in the other alignment media. The addition of negatively charged SDS to the bicelles decreased the overall

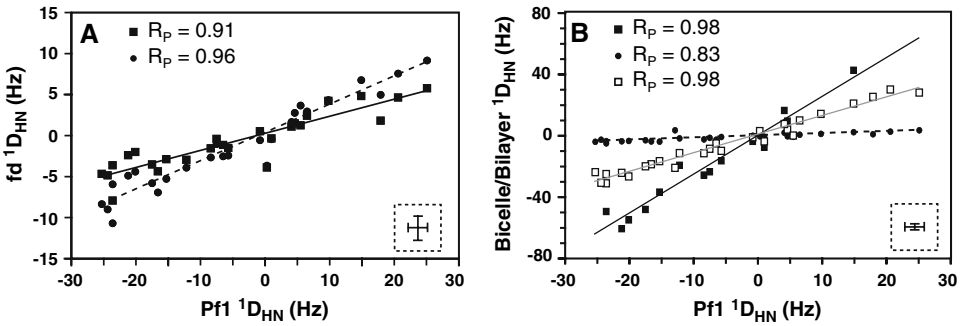

Fig. 2 Scatter plots of experimental one-bond ^{1}H-^{15}N imino $^{1}D_{HN}$ values for native *E. coli* tRNA^{Val} in 10 mg/ml Pf1 bacteriophage plotted against $^{1}D_{HN}$ values in the presence of (**a**) fd or fd-9ah8 bacteriophage and (**b**) bicelle or bilayer alignment media. (**a**) Squares are the $^{1}D_{HN}$ values in wild-type fd and circles are the $^{1}D_{HN}$ values in the longer fd mutant, fd-9ah8. (**b**) Filled squares are the $^{1}D_{HN}$ values in DMPC/DHPC bicelles, filled circles are the $^{1}D_{HN}$ values in SDS-doped DMPC/DHPC bicelles and open squares are the $^{1}D_{HN}$ values in C_8E_5/1-octanol bilayers. The lower right inset of each graph shows error bars representing the ±1.5 Hz error in the $^{1}D_{HN}$ values, and the Pearson's correlation coefficient (R_P) values are given in the upper left of each graph. The lines are the best linear fit for each plot

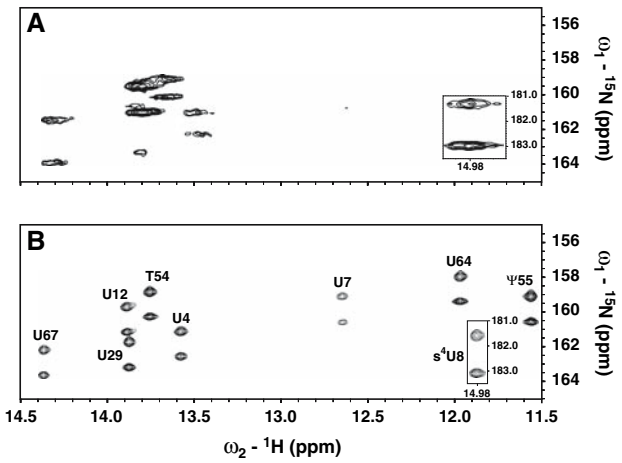

Fig. 3 The uracil imino region from the 2D ^{1}H, ^{15}N doublet selected, sensitivity enhanced HQSC spectra of uniformly ^{15}N-labeled native *E. coli* tRNA^{Val} in (**a**) DMPC/DHPC bicelles and (**b**) SDS-doped DMPC/DHPC bicelles. Spectra were collected at 600 MHz and 38°C. The lower right inset of each spectrum shows the downfield shifted s^{4}U8 imino resonance. Imino assignments for each residue are indicated in (**b**)

magnitude of alignment and thus eliminated the extensive line-broadening (Fig. 3b), yielding 27 measurable $^{1}D_{HN}$ values. The scatter plot of $^{1}D_{HN}$ for Pf1 versus SDS-doped bicelles has a somewhat lower correlation coefficient (R_P = 0.83) than the other plots, but these data still have a strong linear correlation (Fig. 2b). The lower degree of correlation between $^{1}D_{HN}$ values for the SDS-doped bicelles and Pf1 likely arises from the much smaller magnitude of alignment but similar magnitude of error (±1.5 Hz) for the RDCs in the SDS-doped bicelles compared to the other alignment media ($^{1}D_{HN}$ values from −4.9 to 3.6 Hz for the SDS-doped bicelles versus ranges of −31.0 to 30.1, −60.7 to 42.7, −30 to 30.1, −7.9 to 5.8, and −10.7 to 9.2 Hz for the Pf1, DMPC/DHPC bicelles, C_8E_5/1-octanol bilayers, wt-fd and fd-9ah8, respectively, Table S1). This larger relative error (58% and 10% for SDS-doped bicelles and Pf1, respectively) leads to the lower correlation coefficient (R_P = 0.83) for the SDS-doped bicelles than the other alignment media (Table S1). These results illustrate that although it is generally advantageous to have a higher degree of alignment of the macromolecule, too much alignment leads to poor RDC data due to severe line broadening. Thus, there is generally a compromise in the degree of alignment where RDCs are large enough to be precisely measured and not large enough to induce large enough ^{1}H-^{1}H RDCs to cause apparent line-broadening and lower signal-to-noise.

To more directly compare the alignment properties of the different media, the alignment tensors were determined by SVD (Losonczi et al. 1999; Sass et al. 1999) for native *E. coli* tRNA^{Val} in each of the external alignment media. This Monte Carlo approach generates a set of alignment tensors that fit the input structure and RDC data (within error). This analysis employed the model for native *E. coli* tRNA^{Val} previously determined by domain orientation studies (Vermeulen et al. 2005). As previously discussed this model contains structural noise, which arises from assuming A-form conformations for the helical domains in tRNA^{Val} (Vermeulen et al. 2005). The presence of structural noise means that the input errors had to be increased beyond the experimental errors to obtain an adequate number of solutions in the SVD calculations for the external media with larger RDC values (see "Materials and methods"). Table 1 shows the results of the SVD calculations, illustrating that although the magnitude of alignment (D_a) varies greatly in the different external

Table 1 Molecular alignment of native *E. coli* tRNA^{Val} by external alignment media[a]

Media	D_a[b] (Hz)	R[b]	rmsd[c] (Hz)	Q[d]	Normalized scalar product[e]
Pf1 (10 mg/ml)	20.4 ± 1.8	0.62 ± 0.17	2.91	0.19	N/A
C_8E_5/1-octanol (3.5% v/v)	25.6 ± 1.0	0.51 ± 0.04	3.17	0.17	0.95
fd (20 mg/ml)	4.1 ± 0.3	0.58 ± 0.07	1.28	0.38	0.93
fd-9ah8 (20 mg/ml)	7.0 ± 0.7	0.52 ± 0.10	1.89	0.34	0.93
DMPC/DHPC[f] (5% q = 3.5:1)	57.1 ± 2.5	0.35 ± 0.07	5.29	0.18	0.87
DMPC/DHPC/SDS (5% q = 3.5:1:0.06)	3.2 ± 0.3	0.49 ± 0.13	1.64	0.62	0.98

[a] For each of the external alignment media, $^{1}D_{HN}$ and the rigid body minimized structure of native *E. coli* tRNA^{Val} (Vermeulen et al. 2005) were used to determine the molecular alignment tensor by SVD as in the program REDCAT (Valafar and Prestegard 2004)

[b] Standard deviations in D_a and R were calculated from the variation of the principal components in the SVD calculations for each of the various alignment tensors

[c] Average rmsd between experimental and calculated $^{1}D_{HN}$ values

[d] Q represents the quality factor and is the average rmsd normalized by the average magnitude of experimental $^{1}D_{HN}$ (Bax 2003)

[e] Normalized scalar product comparing each of the external alignment media to Pf1 (Sass et al. 1999)

[f] The high degree of alignment in these bicelles led to observation of fewer RDCs than the other media biasing this data set and resulting in less accurate values of the alignment tensor properties (see text)

media, the rhombicity (R) values are generally similar. The size of D_a depends upon the degree of alignment in each of the media and thus does not provide information on the independence of the alignment tensors in different media. Table 1 also shows that the different external media have comparable relative errors for the magnitudes of their alignment tensors (5–10% for D_a and 10–27% for R). The similar relative errors for D_a and R in the various media indicates that the errors introduced to account for structural noise are equal to or greater than the experimental errors in the RDC measurements in these SVD calculations (Zweckstetter and Bax 2002). Thus the SVD calculations likely over estimate the true errors in determining the magnitudes and angles of the alignment tensor.

As mentioned above, there are only half as many observable RDCs for $tRNA^{Val}$ in the DMPC/DHPC bicelles due to the apparent line-broadening arising from the high degree of alignment ($D_a = \sim 57$ Hz). It is also important to note that a many of the RDCs with the largest magnitudes in the other media were not observed in the DMPC/DHPC bicelles (Fig. 2b and Table S1). Thus the 14 observable imino RDCs in the bicelle medium represent a limited and highly biased data set compared to the RDCs measured in the other alignment media. The inability to measure the largest RDCs in the DMPC/DHPC bicelles leads to systematic errors in calculating the alignment tensor for $tRNA^{Val}$ in this medium. However, the remaining RDCs are still highly correlated with the Pf1 RDCs ($R_P = 0.98$; Fig. 2b), indicating that the RDCs for the bicelles would not provide an independent alignment tensor from that observed for Pf1. Thus, the smaller R for $tRNA^{Val}$ in the DMPC/DHPC bicelles cannot be interpreted as a different alignment tensor for this medium, but reflects inaccurate estimates for the principal components of the alignment tensor due to limited and biased sampling of the RDC data in this medium (see below).

Table 1 also shows that all of these alignment media yielded rather similar qualities of fit, Q, to the structure of $tRNA^{Val}$ (average rmsd = 1.28–5.29 Hz and $Q = 0.17$–0.62). Q is the average rmsd normalized by the average magnitude of the measured RDCs and allows comparison of RDC data sets even with very different D_a values (Bax 2003). Part of the Q values (and average rmsd) are due to structural noise resulting from deviations in the local structure of the tRNA away from the assumed A-form conformation (Zweckstetter and Bax 2002; Vermeulen et al. 2005). Since Q directly compares the experimental RDC values to back-calculated values, it is also sensitive to the experimental error, and the RDCs generated from alignment media with the largest relative errors have the largest Q values (Table 1). To further assess the independence of the alignment tensors for tRNA in the different alignment media, the normalized scalar product was calculated for each tensor relative to the tensor for Pf1 phage. This scalar product is the cosine of the angle between two tensors and provides an estimate of the co-linearity of the two alignment tensors (Sass et al. 1999), where a scalar product of 1 means exact co-linearity for the two tensors. With the exception of the DMPC/DHPC medium, which has an inaccurate alignment tensor (see above), the normalized scalar product ranges from 0.93 to 0.98 between the different alignment media and Pf1, indicating a high degree of co-linearity between the alignment tensors (Table 1).

The Sauson-Flaumsteed projection maps obtained from the SVD analysis (Fig. 4) can also be used to compare the orientations of principal components of the alignment

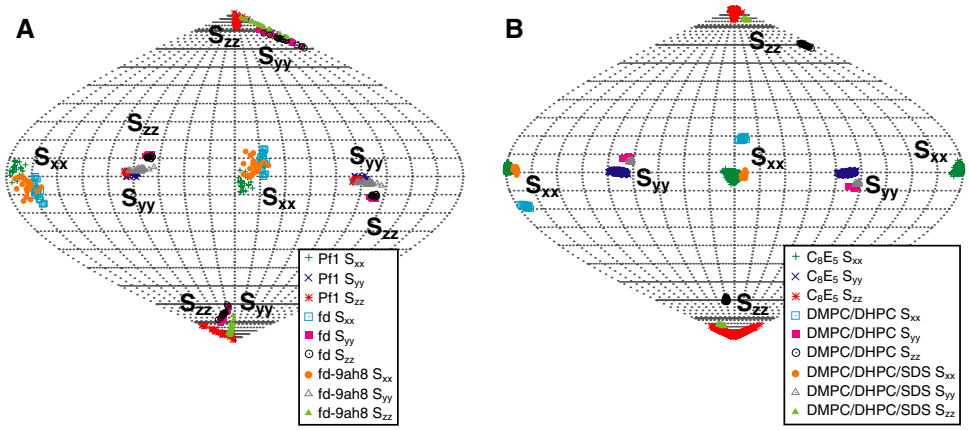

Fig. 4 Sauson-Flaumsteed projection maps illustrating the orientations of the principal components of the molecular alignment tensor for native *E. coli* $tRNA^{Val}$ derived from alignment by (**a**) various filamentous bacteriophage and (**b**) bilayer or bicelle alignment media. The positions of the principal components S_{xx}, S_{yy} and S_{zz} of the alignment are indicated on each map. The legend in the lower right of each map shows the symbols for the principal components for the various alignment media. Due to the high rhombicity for several of the alignment tensors, the orientations of S_{zz} and S_{yy} are exchanged. Sauson-Flaumsteed projection maps were generated from the SVD output using the program REDCAT (Valafar and Prestegard 2004). Fifty solutions are plotted for each alignment tensor

tensor (where $|S_{zz}| \geq |S_{yy}| \geq |S_{xx}|$) for tRNA^{Val} in the different alignment media. These maps were referenced such that the S_{zz} component of tRNA^{Val} for the Pf1 phage is oriented at the top (or the bottom) of the globe. The alignment tensor of the tRNA^{Val} in Pf1 has a high rhombicity (Table 1), which means that the S_{zz} and S_{yy} components of the alignment tensors have similar magnitudes. This is manifested in the Sauson-Flaumsteed projection maps where some members of the set of alignment tensors consistent with the input data have exchanged orientations of the S_{zz} and S_{yy} components (Fig. 4a). This property is a natural consequence of the high rhombicity of tRNA^{Val} alignment in the various alignment media. Excluding the biased DMPC/DHPC data, the Sauson-Flaumsteed projection maps for the other external alignment media show similar orientations for the components of the alignment tensors. Given that the various alignment media have different relative errors in their RDC data, it is unexpected that the maps show a similar variation in the orientation of their alignment tensor components. However, this similar variation is a direct consequence of the larger input error required to account for the structural noise in the SVD calculations for some of the alignment media (see "Materials and methods"). As noted above, the DMPC/DHPC data yields an inaccurate alignment tensor for tRNA^{Val}. This is further illustrated in Fig. 4b where there is a $\sim$20° difference in the orientation for S_{zz} compared to the other media. To demonstrate that this difference in orientation results from the biased set of RDCs for the DMPC/DHPC medium, the RDCs that were not observed in the DMPC/DHPC data set were removed from the Pf1 and C_8E_5/1-octanol data sets. The SVD calculations on these data sets also have S_{zz} shifted by $\sim$15–20° and smaller R (data not shown), demonstrating that the RDC data for the DMPC/DHPC medium leads to an inaccurate alignment tensor.

It is not surprising that these different alignment media give similar alignment tensors for tRNA^{Val}. Previous studies of the mechanisms of alignment of macromolecules in liquid crystalline media have shown that molecular alignment tensors in liquid crystalline media can be accurately predicted using a steric obstruction model (Zweckstetter and Bax 2000) or a mixed steric obstruction and electrostatic repulsion model (Zweckstetter et al. 2004). Wu et al. (2006) have also recently developed an analytical approach employing the Debye-Huckel approximation for electrostatic repulsion to predict the alignment tensors of nucleic acids in Pf1. The combined results of these studies predict that alignment of nucleic acids under conditions of electrostatic repulsion is functionally the same as alignment under conditions of steric exclusion (Zweckstetter and Bax 2000; Zweckstetter et al. 2004; Wu et al. 2006). These theoretical predictions are experimentally observed in the results presented here for tRNA^{Val} (Figs. 2 and 4 and Table 1), where the alignment of tRNA^{Val} is essentially the same in negatively charged (Pf1 phage, fd phage and SDS-doped bicelles) and in neutral (bicelles and bilayers) liquid crystalline media. Thus a different alignment mechanism, besides steric or electrostatic repulsion, needs to be employed to obtain an independent alignment tensor in tRNA^{Val}.

Magnetic alignment of *E. coli* native tRNA^{Val}

In an attempt to generate a different alignment tensor, the one-bond ^{1}H-^{15}N imino couplings were measured at four magnetic fields and used to determine the MSA-induced $^1D_{HN}$(800) and $^1D_{HN}$(900) values for tRNA^{Val} (Table S2). As seen in the scatter plot in Fig. 5 these $^1D_{HN}$ values do not correlate as well with the $^1D_{HN}$ for Pf1 as the $^1D_{HN}$ values for the other alignment media (R_P = 0.77 and 0.79 for $^1D_{HN}$ data at 800 and 900 MHz, respectively). A scatter plot of the $^1D_{HN}$ values at 800 and 900 MHz yielded a higher R_P of 0.95 (data not shown) indicating the lower R_P values in the plots with Pf1 are not simply a result of larger relative errors in measurement of the MSA-induced RDCs compared to the errors in the external alignment media (which have relative errors of 72%, 74% and 10% for $^1D_{HN}$(800), $^1D_{HN}$(900) and Pf1, respectively). The $^1D_{HN}$ values at 800 and 900 MHz were normalized, averaged and used as input for SVD analysis with the same tRNA^{Val} model that was employed for the external media above (Vermeulen et al. 2005). These MSA-induced RDCs fit

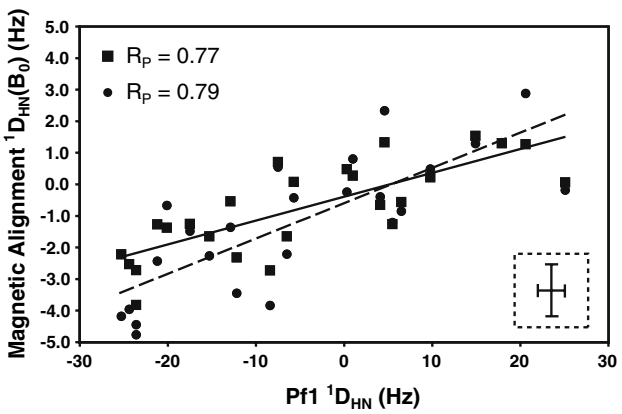

Fig. 5 Scatter plot of the experimental $^1D_{HN}$ values of native *E. coli* tRNA^{Val} in 10 mg/ml Pf1 plotted against $^1D_{HN}$ values for magnetic alignment at 800 MHz (filled squares) and 900 MHz (filled circles). The solid and dashed lines correspond to the best-fit line of the Pf1 data to the 800 and 900 MHz data, respectively. The lower right inset shows an error bar representing the ±1.5 and ±0.8 Hz errors in the $^1D_{HN}$ values obtained from Pf1 and MSA-induced alignment, respectively, and the R_P values are given in the upper left of each graph. The lines are the best linear fit for each plot

well to the structure of $tRNA^{Val}$ (Q = 0.45 and average rmsd = 0.72 Hz). Magnetic alignment produces only a small degree of ordering for $tRNA^{Val}$ (D_a = −2.0 Hz at 800 MHz), along with a somewhat smaller rhombicity than alignment with Pf1 (R = 0.42 vs. 0.62). Even though $tRNA^{Val}$ has 76 nucleotides, it has only a small degree of alignment at 900 MHz due to partial cancellation of the individual nucleobase magnetic anisotropies (Ying et al. 2007) arising from the ~90° orientation of the anticodon arm and acceptor arm in $tRNA^{Val}$ (Mollova et al. 2000). The normalized scalar product of the two alignment tensors of $tRNA^{Val}$ generated by magnetic alignment and Pf1 alignment is 0.94, indicating a high degree of co-linearity. This suggests that MSA-induced alignment and external alignment media do not generate independent alignment tensors. Figure 6 compares the Sauson-Flaumsteed maps depicting the orientations of the principal components of the alignment tensor for the Pf1 phage data and the $^1D_{HN}$(800, 900) data for MSA-induced alignment of $tRNA^{Val}$. The relative magnitudes and orientations of the principal axes for the Pf1 and MSA-induced alignment are also shown in Fig. 7, referenced to the structural model for $tRNA^{Val}$. Again, the large rhombicity of the Pf1 alignment tensor is highlighted pictorially in Fig. 7 (red axis system), which shows that S_{zz} and S_{yy} for Pf1 alignment have similar magnitudes. These figures also illustrate that the S_{zz} axis for the MSA-induced alignment tensor is rotated by ~95° relative to the S_{zz} axis for Pf1 and is nearly co-linear with S_{yy} for Pf1. Finally, S_{xx} for both alignment tensors are in a similar orientation. The magnetic susceptibility of the nucleobases in an A-form RNA helix leads to the helical axis being oriented roughly perpendicular to the applied magnetic field, which is in contrast to the external media where the helical axis is oriented parallel to the magnetic

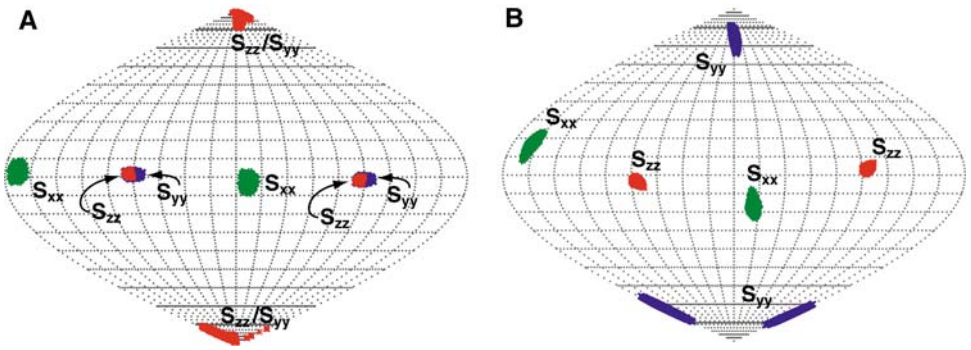

Fig. 6 Sauson-Flaumsteed projection maps illustrating the orientations of the principal components of the molecular alignment tensor derived from alignment by (**a**) 10 mg/ml Pf1 and (**b**) MSA-induced alignment using the normalized average RDC values measured at 800 and 900 MHz, $^1D_{HN}$(800, 900). Areas of green, blue and red correspond to the orientations of the principal components of the order tensor S_{xx}, S_{yy}, and S_{zz}, respectively

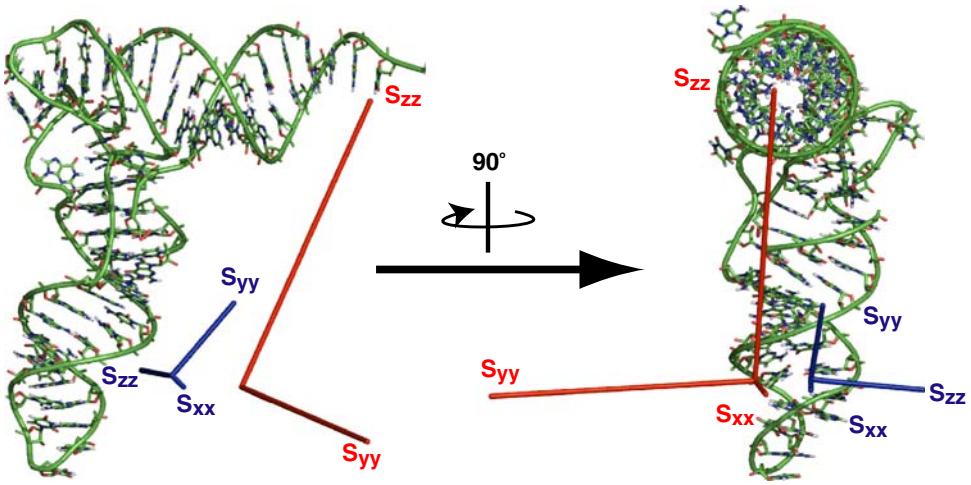

Fig. 7 Relative orientations of the principal components of the molecular alignment tensors for native *E. coli* $tRNA^{Val}$ resulting from Pf1 (red) and MSA-induced alignment (blue). The magnitude and orientation of S_{xx}, S_{yy} and S_{zz} were determined by SVD analysis of the $^1D_{HN}$ values using the program REDCAT. The lengths of S_{xx}, S_{yy}, and S_{zz} represent their magnitudes and are relative to the S_{zz} for Pf1 alignment. For visualization purposes, the lengths of S_{xx}, S_{yy}, and S_{zz} for the MSA-induced alignment tensor are amplified 5-fold

field. Typically, the S_{zz} of the MSA-induced alignment tensor is oriented along the helical axis; however, the L-shape of tRNA not only reduces MSA-induced alignment but also leads to S_{zz} being oriented perpendicular to the plane of the L (Fig. 7, blue axis system).

The $\sim$95° shift of S_{zz} for the MSA-induced indicates a different alignment tensor for $tRNA^{Val}$ compared to that obtained in Pf1. However, as discussed above, the relatively high rhombicity of the alignment tensor in Pf1 phage also leads to a set of alignment tensors from the SVD analysis with S_{zz} being rotated by 90°, which is in a similar orientation as the alignment tensor for the MSA-induced alignment (Figs. 6 and 7). Thus the experimental results show that MSA-induced alignment of native $tRNA^{Val}$ generates a different, but not an independent, alignment tensor from the ones generated by the various external alignment media.

Eliminating degeneracy in domain orientations of tRNA using RDC data

One reason for developing different methods for partially aligning macromolecules is that RDCs measured from two (or more) independent alignment tensors greatly simplify domain orientation studies (Al-Hashimi et al. 2000, 2001; Lipsitz and Tjandra 2004). Thus SVD calculations were performed to test if combining RDC data from magnetic alignment and external alignment could eliminate the orientational degeneracy observed in the studies of $tRNA^{Val}$ (Mollova et al. 2000; Vermeulen et al. 2005). For these calculations the model $tRNA^{Val}$ structure was rotated into the principal axis system of the Pf1 alignment tensor and separated into two helical domains, the anticodon arm and the acceptor arm (Fig. 1). The anticodon arm was independently rotated by 180° about the *x*-, *y*-, or *z*-axis of the principal axis system to generate four structures. These four structures represent the four degenerate solutions for orienting two domains using RDC data from one external alignment medium (Bruschweiler et al. 1995). The $^1D_{HN}(800, 900)$ values were then used as SVD input for each of the four structures. As seen in Table 2, two of the four structures have higher *Q* factors, indicating that these orientations yield poorer fits to the experimental magnetic alignment RDCs. However, all four structures have *Q* factors (Q = 0.44–0.62) within the range seen for fitting the experimental RDCs for the various external alignment media (Tables 1 and 2). Thus the MSA-induced RDC data might be able to rule out two of the structures, but the other two fit equally well. The RNA covalent structure and steric overlap also eliminates two of the possible orientations for $tRNA^{Val}$ (structures 2 and 3) (Mollova et al. 2000), but these are the same structures eliminated based on the higher *Q* factors. Thus to determine if the high relative error of the MSA-induced RDCs is the cause for the similar *Q* factors for structures 1 and 4, SVD calculations were performed with simulated (error free) RDCs to determine if it is possible to eliminate the orientation degeneracy by using perfectly accurate and precise MSA-induced $^1D_{HN}(800)$ data. These SVD calculations employed 21 $^1D_{HN}(800)$ values that were predicted for the imino RDCs used in the SVD analysis with the experimental MSA data

Table 2 SVD analysis of MSA-induced RDCs

	Domain orientation degenerate structures[a]			
	1	2	3	4
Axis of rotation	N/A	*x*	*y*	*z*
Q	Experimental $^1D_{HN}(800, 900)$			
	0.44	0.62	0.65	0.44
Q	Predicted RDCs from observed imino resonances[b]			
	0.01	0.60	0.61	0.18
Q	Predicted RDCs from rotated alignment tensor[c]			
	0.00	0.59	0.36	0.52

[a] $tRNA^{Val}$ structures generated by separating the RNA structure into two domains and rotating the anticodon arm domain (residues 10–13 and 22–43, Fig. 1) around the indicated axis of the Pf1 alignment tensor. Structure 1 is the original structure (Vermeulen et al. 2005) whereas structures 2, 3 and 4 involve rotations around the *x*, *y* and *z* axes, respectively

[b] The MSA-induced alignment tensor for structure 1 was modeled using the method of Bryce et al. (2004). A set of 21 RDC values were predicted based on this alignment tensor and structure 1. These RDC values were then used in SVD analysis for the four orientationally degenerate structures of $tRNA^{Val}$

[c] The modeled MSA-induced alignment tensor (in b) was modified where S_{zz} was rotated by $\sim$45°. A new set of 21 RDC values were predicted based on this alignment tensor and structure 1. These RDC values were then also used in SVD analysis for the four orientationally degenerate structures of $tRNA^{Val}$

discussed above. The $^1D_{HN}(800)$ values were generated from the $tRNA^{Val}$ model using a predicted alignment tensor for MSA-induced alignment (Bryce et al. 2004), which is calculated by summing the magnetic anisotropy tensors of all the individual bases. These predicted $^1D_{HN}(800)$ values were used as SVD input with each of the four orientationally degenerate $tRNA^{Val}$ structures. Table 2 shows that using these perfectly accurate and precise MSA-induced RDC data, it is possible to eliminate the 4-fold degeneracy. The Q factors for structures 2 and 3 are much larger than the Q factor for structures 1 and 4 and would likely rule out these structures for real experimental data. However, even though the Q for structure 4 is higher than for the correct structure 1, it is still quite small ($Q = 0.18$). Thus structural noise in the domain orientation analysis (Zweckstetter and Bax 2002; Vermeulen et al. 2005) and measurement errors in experimental RDCs would generally make it impossible to distinguish between structures 1 and 4 for real experimental data.

To test whether a more complete set of RDC data would eliminate the orientational degeneracy in the domain orientation studies of $tRNA^{Val}$, additional $^1D_{HN}(800)$ values were predicted for imino groups in the anticodon arm and included in the SVD analysis of the MSA-induced alignment. There are fewer experimental imino RDC data for the anticodon arm compared to the acceptor arm (8 vs. 13), thus these calculations test whether including more experimental RDCs for the anticodon arm can eliminate the orientational degeneracy. The predicted $^1D_{HN}(800)$ values for imino proton groups for residues U33, U34, G43, G44 and G45 in the anticodon arm (Fig. 1a) were included in these SVD calculations. These imino proton resonances were not experimentally observed for $tRNA^{Val}$, presumably due to rapid proton exchange with water. These additional data lead to very small changes in the Q factors (data not shown). Thus including a more complete set of the imino RDC data does not eliminate the 2-fold degeneracy for the domain orientation studies of $tRNA^{Val}$.

The alignment tensor for MSA-induced alignment of $tRNA^{Val}$ has S_{zz} rotated by $\sim 95°$ relative to the S_{zz} observed for alignment with Pf1 (Figs. 6 and 7), and as noted above this leads to little independence of the MSA-induced RDC data due to the high rhombicity of the Pf1 tensor. To test if RDC data for a different orientation of the MSA-induced alignment tensor could eliminate the orientational degeneracy in the domain orientation studies, a set of 21 RDCs was predicted using the same magnitudes but different orientations of the principal components of the MSA-induced alignment tensor. In these simulations the S_{zz} axis of the MSA-induced alignment was rotated by $\sim 45°$ relative to the Pf1 data. As seen in Table 2, it is possible to eliminate two of the four possible structures (2 and 4) based on the higher Q factors. Whether structure 3 can be eliminated based on Q-factor alone will depend upon the level of structural noise and experimental error; however, this solution is eliminated due to steric overlap (Mollova et al. 2000). Al-Hashimi et al. (2001) employed the combination of Pf1 and MSA-induced alignment to orient two domains in a homodimeric DNA quadraplex with C2 symmetry. Similar to what was observed here, the MSA-induced alignment was able to rule out two of the four degenerate solutions. However, in that system the two remaining solutions are related by rotation about the C2 axis of symmetry inherent in the DNA homodimer (Al-Hashimi et al. 2001). Thus a unique domain orientation was obtained for this system because the molecule contains a C2 axis of symmetry. These results demonstrate that, in optimal cases, it is possible to combine RDC data from external alignment media and magnetic alignment to uniquely orient two domains in nucleic acids. Another potential approach for generating different alignment tensors for tRNA is the use of paramagnetic tags, where an attached paramagnetic metal induces molecular alignment (Rodriguez-Castaneda et al. 2006). In the absence of an independent alignment tensor, additional data, such as steric overlap or NOE constraints (Mollova et al. 2000; Bondensgaard et al. 2002), need to be used to eliminate the orientational degeneracy obtained in domain orientation studies of RNAs.

Acknowledgments We thank Gabe Gittings for purification of the fd and fd mutant bacteriophage, Dr. Jinfa Ying for advice in acquiring the NMR spectra for magnetic alignment, Dr. Alexander Grishaev for the FORTRAN program for calculating the MSA-induced alignment tensor and Dr. Ad Bax for critical advice in collection of the MSA-induced RDCs and for valuable discussions. This work is supported in part by NIH grant AI33098, and MPL was supported in part by a NIH training grant T32 GM65103. The NMR instrumentation was purchased with partial support from NIH grants RR11969, RR16649 and GM068928, NSF grants 9602941 and 0230966, and the W. M. Keck Foundation.

References

Al-Hashimi HM, Valafar H, Terrell M, Zartler ER, Eidsness MK, Prestegard JH (2000) Variation of molecular alignment as a means of resolving orientational ambiguities in protein structures from dipolar couplings. J Magn Reson 143:402–406

Al-Hashimi HM, Majumdar A, Gorin A, Kettani A, Skripkin E, Patel DJ (2001) Field- and phage-induced dipolar couplings in a homodimeric DNA quadruplex, relative orientation of G·(C-A) triad and G-tetrad motifs and direct determination of C2 symmetry axis orientation. J Am Chem Soc 123:633–640

Amiri KMA, Hagerman PJ (1994) Global conformation of a self-cleaving hammerhead RNA. Biochemistry 33:13172–13177

Bax A (2003) Weak alignment offers new NMR opportunities to study protein structure and dynamics. Protein Sci 12:1–16

Bax A, Kontaxis G, Tjandra N (2001) Dipolar couplings in macromolecular structure determination. Methods Enzymol 339:127–174

Bondensgaard K, Mollova ET, Pardi A (2002) The global conformation of the hammerhead ribozyme determined using residual dipolar couplings. Biochemistry 41:11532–11542

Bothner-By AA (1995) In: Grant DM, Harris RK (eds) Encyclopedia of nuclear magnetic resonance. Wiley, Chichester, pp 2932–2938

Bruschweiler R, Liao XB, Wright PE (1995) Long-range motional restrictions in a multidomain zinc-finger protein from anisotropic tumbling. Science 268:886–889

Bryce DL, Boisbouvier J, Bax A (2004) Experimental and theoretical determination of nucleic acid magnetic susceptibility: importance for the study of dynamics by field-induced residual dipolar couplings. J Am Chem Soc 126:10820–10821

Clore GM, Starich MR, Gronenborn AM (1998) Measurement of residual dipolar couplings of macromolecules in the nematic phase of a colloidal suspension of rod-shaped viruses. J Am Chem Soc 120:10571–10572

Cordier F, Dingley AJ, Grzesiek S (1999) A doublet-separated sensitivity-enhanced HSQC for the determination of scalar and dipolar one-bond J-couplings. J Biomol NMR 13:175–180

Davis JH, Tonelli M, Scott LG, Jaeger L, Williamson JR, Butcher SE (2005) RNA helical packing in solution: NMR structure of a 30 kDa GAAA tetraloop-receptor complex. J Mol Biol 351:371–382

Delaglio F, Grzesiek S, Vuister GW, Zhu G, Pfeifer J, Bax A (1995) NMRPipe: a multidimensional spectral processing system based on UNIX pipes. J Biomol NMR 6:277–293

Friederich MW, Hagerman PJ (1997) The angle between the anticodon and aminoacyl acceptor stems of yeast tRNA(Phe) is strongly modulated by magnesium ions. Biochemistry 36:6090–6099

Gayathri C, Bothner-By AA, Vanzijl PCM, Maclean C (1982) Dipolar magnetic-field effects in NMR-spectra of liquids. Chem Phys Lett 87:192–196

Getz M, Sun X, Casiano-Negroni A, Zhang Q, Al-Hashimi HM (2007) Review NMR studies of RNA dynamics and structural plasticity using NMR residual dipolar couplings. Biopolymers 86:384–402

Hansen MR, Mueller L, Pardi A (1998) Tunable alignment of macromolecules by filamentous phage yields dipolar coupling interactions. Nat Struct Biol 5:1065–1074

Hansen MR, Hanson P, Pardi A (2000) Filamentous bacteriophage as a versatile method for aligning RNA, DNA and proteins for measurement of NMR dipolar coupling interactions. Methods Enzymol 317:220–240

Latham MP, Brown DJ, McCallum SA, Pardi A (2005) NMR methods for studying the structure and dynamics of RNA. Chembiochem 6:1492–1505

Lilley DM (2004) Analysis of global conformational transitions in ribozymes. Methods Mol Biol 252:77–108

Lipsitz RS, Tjandra N (2004) Residual dipolar couplings in NMR structure analysis. Annu Rev Biophys Biomol Struct 33:387–413

Losonczi JA, Prestegard JH (1998) Improved dilute bicelle solutions for high-resolution NMR of biological macromolecules. J Biomol NMR 12:447–451

Losonczi JA, Andrec M, Fischer MW, Prestegard JH (1999) Order matrix analysis of residual dipolar couplings using singular value decomposition. J Magn Reson 138:334–342

Lukavsky PJ, Kim I, Otto GA, Puglisi JD (2003) Structure of HCV IRES domain II determined by NMR. Nat Struct Biol 10:1033–1038

Mollova ET, Hansen MR, Pardi A (2000) Global structure of RNA determined with residual dipolar couplings. J Am Chem Soc 122:11561–11562

Padrta P, Stefl R, Kralik L, Zidek L, Sklenár V (2002) Refinement of d(GCGAAGC) hairpin structure using one- and two-bond residual dipolar couplings. J Biomol NMR 24:1–14

Pervushin K, Riek R, Wider G, Wüthrich K (1997) Attenuated T2 relaxation by mutual cancellation of dipole-dipole coupling and chemical shift anisotropy indicates an avenue to NMR structures of very large biological macromolecules in solution. Proc Natl Acad Sci U S A 94:12366–12371

Piotto M, Saudek V, Sklenár V (1992) Gradient-tailored excitation for single-quantum NMR-spectroscopy of aqueous-solutions. J Biomol NMR 2:661–665

Ramirez BE, Bax A (1998) Modulation of the alignment tensor of macromolecules dissolved in a dilute liquid crystalline medium. J Am Chem Soc 120:9106–9107

Richards RJ, Wu H, Trantirek L, O'Connor CM, Collins K, Feigon J (2006) Structural study of elements of tetrahymena telomerase RNA stem-loop IV domain important for function. RNA 12:1475–1485

Rodriguez-Castaneda F, Haberz P, Leonov A, Griesinger C (2006) Paramagnetic tagging of diamagnetic proteins for solution NMR. Magn Reson Chem 44 Spec No: S10–S16

Ruckert M, Otting G (2000) Alignment of biological macromolecules in novel nonionic liquid crystalline media for NMR experiments. J Am Chem Soc 122:7793–7797

Sass J, Cordier F, Hoffmann A, Cousin A, Omichinski JG, Lowen H, Grzesiek S (1999) Purple membrane induced alignment of biological macromolecules in the magnetic field. J Am Chem Soc 121:2047–2055

Sass HJ, Musco G, Stahl SJ, Wingfield PT, Grzesiek S (2000) Solution NMR of proteins within polyacrylamide gels: diffusional properties and residual alignment by mechanical stress or embedding of oriented purple membranes. J Biomol NMR 18:303–309

Staple DW, Butcher SE (2003) Solution structure of the HIV-1 frameshift inducing stem-loop RNA. Nucleic Acids Res 31:4326–4331

Tjandra N, Bax A (1997) Direct measurement of distances and angles in biomolecules by NMR in a dilute liquid crystalline medium. Science 278:1111–1114

Tolman JR, Flanagan JM, Kennedy MA, Prestegard JH (1995) Nuclear magnetic dipole interactions in field-oriented proteins: information for structure determination in solution. Proc Natl Acad Sci U S A 92:9279–9283

Tycko R, Blanco FJ, Ishii Y (2000) Alignment of biopolymers in strained gels: a new way to create detectable dipole-dipole couplings in high-resolution biomolecular NMR. J Am Chem Soc 122:9340–9341

Valafar H, Prestegard JH (2004) REDCAT: a residual dipolar coupling analysis tool. J Magn Reson 167:228–241

van Buuren BNM, Schleucher A, Wittmann V, Griesinger C, Schwalbe H, Wijmenga SS (2004) NMR spectroscopic determination of the solution structure of a branched nucleic acid from residual dipolar couplings by using isotopically labeled nucleotides. Angewandte Chemie-Int Ed 43:187–192

Vermeulen A (2003) Determining nucleic acid global structure by application of NMR residual dipolar couplings. Dissertation, University of Colorado

Vermeulen A, Zhou H, Pardi A (2000) Determining DNA global structure and DNA bending by application of NMR residual dipolar couplings. J Am Chem Soc 122:9638–9647

Vermeulen A, McCallum SA, Pardi A (2005) Comparison of the structure and dynamics of native and unmodified $tRNA^{val}$. Biochemistry 44:6024–6033

Wu B, Petersen M, Girard F, Tessari M, Wijmenga SS (2006) Prediction of molecular alignment of nucleic acids in aligned media. J Biomol NMR 35:103–115

Ying J, Grishaev A, Latham MP, Pardi A, Bax A (2007) Magnetic field induced residual dipolar couplings of imino groups in

nucleic acids from measurements at a single magnetic field. J Biomol NMR 39:91–96

Yue D (1994) Structure and function of unmodified *E. coli* valine-tRNA. Dissertation, Iowa State University

Zweckstetter M, Bax A (2000) Prediction of sterically induced alignment in a dilute liquid crystalline phase: aid to protein structure determination by NMR. J Am Chem Soc 122:3791–3792

Zweckstetter M, Bax A (2002) Evaluation of uncertainty in alignment tensors obtained from dipolar couplings. J Biomol NMR 23: 127–137

Zweckstetter M, Hummer G, Bax A (2004) Prediction of charge-induced molecular alignment of biomolecules dissolved in dilute liquid-crystalline phases. Biophys J 86:3444–3460